

# Optimized Pulse Patterns for Five-Level Medium-Voltage Drives With DC-Link Voltage Ripple Minimization

Ilari Hilden

*Faculty of Inf. Technol. and Commun. Sciences*  
Tampere University  
Tampere, Finland  
ilari.hilden@tuni.fi

Petros Karamanakos

*Faculty of Inf. Technol. and Commun. Sciences*  
Tampere University  
Tampere, Finland  
p.karamanakos@ieee.org

Tobias Geyer

*Motion System Drives*  
ABB Switzerland Ltd  
Turgi, Switzerland  
t.geyer@ieee.org

**Abstract**—This paper presents a control strategy for medium-voltage (MV) drives based on a five-level neutral-point-clamped (NPC) H-bridge inverter and a 36-pulse diode rectifier. The proposed method leverages optimized pulse patterns (OPPs) to achieve superior steady-state performance compared to conventional approaches. Specifically, tailored OPPs are employed that effectively suppress the significant dc-link voltage ripple, including the dominant second harmonic, which is inherent to the five-level NPC H-bridge topology. This is accomplished by performing harmonic analysis of the dc-link voltage and formulating an OPP optimization problem that minimizes its harmonic content, while bounding the stator current harmonic distortion to ensure load-friendly operation. To enable high-bandwidth control, a model predictive control (MPC) strategy adjusts the OPP switching time instants in real time. As a result, fast transient responses and excellent disturbance rejection are achieved. The effectiveness of the proposed approach is demonstrated through system-level simulations, with performance comparisons highlighting its advantages over conventional methods.

**Index Terms**—Model predictive control (MPC), optimized pulse patterns (OPPs), medium-voltage (MV) drives, multilevel converters

## I. INTRODUCTION

In medium-voltage (MV) drives, multilevel power converters are commonly used due to their ability to reduce harmonic distortions and lower the stress on the semiconductor devices compared to the traditional two-level converter [1]. One such topology used in industrial MV drives is the five-level neutral-point-clamped (NPC) H-bridge inverter, which consists of cascaded three-level H-bridge modules [2]. However, this configuration requires an independent dc link for each phase, leading to a dominant second harmonic in the dc-link voltages due to single-phase power draw. Such a significant oscillation in the dc link can degrade the stator current quality and unduly stress the switching devices [3]. A further challenge of this topology is that it must operate at switching frequencies of only a few hundred hertz to reduce the switching losses and preserve the high-power capability of the inverter [4]. However, the performance of conventional modulation methods, such as carrier-based pulse width modulation (CB-PWM), deteriorates at such low switching frequencies. As a result, the

current distortions are increased and, consequently, the thermal losses in the machine.

Considering the above, optimized pulse patterns (OPPs) provide a promising solution to the aforementioned challenges [5], [6]. OPPs are a PWM technique where a mathematical optimization problem is formulated and solved offline. The result of the optimization process, namely the optimal switching signal, characterized by the switching angles (i.e., switching time instants) and structure of the pattern, is stored in a look-up-table (LUT). Conventionally, the optimization problem is designed to minimize the harmonic distortions in the load current—e.g., the stator current when a machine is considered—quantified by its total demand distortion (TDD). Hence, OPPs can produce high-quality currents even at low switching-to-fundamental frequency ratios [7]. More interestingly, in addition to this capability, additional objectives and constraints can be incorporated into the optimization problem, enabling OPPs to tackle system-specific challenges [8].

To fully leverage the mentioned advantages of OPPs, this paper computes tailored OPPs for the five-level NPC H-bridge drive that not only minimize the stator current TDD—as conventional OPPs do—but also effectively reduce the ripple in the dc-link voltages. To this end, the harmonic content of the dc-link voltage is derived as a function of the to-be-computed switching angles and inverter output voltage levels. By doing so, an OPP optimization problem that aims at minimizing the dc-link voltage harmonic content is formulated. The additional objective of low current harmonic distortions is achieved by adding an explicit inequality constraint on the stator current TDD. Hence, by choosing the upper bound on the current TDD, a favorable trade-off between current distortions and dc-link voltage ripple is achieved.

Finally, to control the drive with the proposed OPPs, a single-phase formulation variant of the gradient-based predictive pulse pattern control algorithm—hereafter referred to as S-GP<sup>3</sup>C—is employed [9]. This algorithm combines direct model predictive control (MPC) [10] with OPPs, leveraging both the high bandwidth of MPC and the favorable characteristics of OPPs. As a result, S-GP<sup>3</sup>C achieves fast transient re-

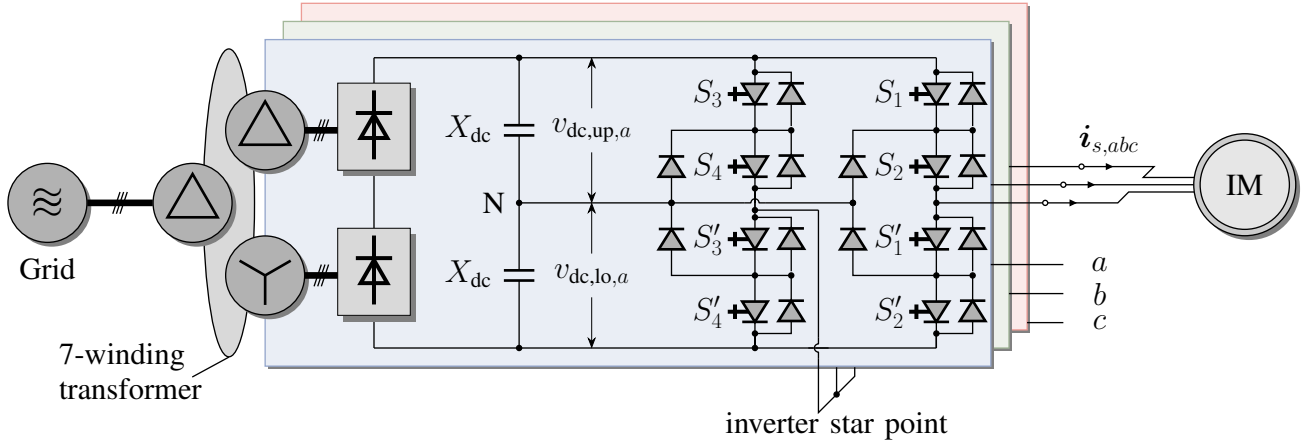


Fig. 1. MV drive with a 36-pulse diode rectifier, a five-level NPC H-bridge inverter, and an induction machine.

sponses and effectively compensates for external disturbances, while also providing excellent steady-state performance.

## II. MATHEMATICAL MODEL OF THE FIVE-LEVEL NPC H-BRIDGE DRIVE

Consider the five-level NPC H-bridge drive system shown in Fig. 1. Each phase of the system features a 12-pulse diode rectifier, supplying two identical dc-link capacitors with reactance  $X_{dc}$ . The dc link feeds each phase of the inverter, which comprises an H-bridge module consisting of two three-level NPC legs. The central point of each NPC leg can be connected to three different potentials, i.e., the negative rail, the neutral point, and the positive rail. As a result, the inverter output voltage in phase  $x$ ,  $x \in \{a, b, c\}$ , can assume five distinct values, namely  $\pm v_{dc,x}$ ,  $\pm v_{dc,x}/2$ , and 0, where  $v_{dc,x} = v_{dc,up,x} + v_{dc,lo,x}$  is the total dc-link voltage for phase  $x$ , see Fig. 1. These output voltage levels are modeled by an integer variable, i.e., the single-phase *switch position*  $u_x \in \{0, \pm 1, \pm 2\}$ , where  $u_x = 0$  denotes that the zero voltage is applied at the output, while  $u_x = \pm 1$  and  $u_x = \pm 2$  indicate that the positive (negative) half- or the positive (negative) full dc-link voltage is applied at the output terminals, respectively.

The single-phase switch position is realized by selecting the single-phase *switching state*  $s_x = [S_1 S_2 S_3 S_4]^T$  with  $S_i \in \{0, 1\}$  denoting the state of the  $i^{\text{th}}$  switching device, where  $i \in \{1, 2, 3, 4\}$ . Given the single-phase switching state  $s_x$ , the stator voltage in phase  $x$  is

$$v_{s,x} = (v_{dc,up,x}[1 \ 0 \ -1 \ 0] + v_{dc,lo,x}[0 \ 1 \ 0 \ -1])s_x. \quad (1)$$

Subsequently, the dynamics of the MV drive system are described by the set of differential equations [11], [12]

$$\frac{di_s}{dt} = -\frac{1}{\tau_s}i_s + \left( \frac{1}{\tau_r} - \omega_r \begin{bmatrix} 0 & -1 \\ 1 & 0 \end{bmatrix} \right) \frac{X_m}{D} \psi_r + \frac{X_r}{D} v_s, \quad (2a)$$

$$\frac{d\psi_r}{dt} = \frac{X_m}{\tau_r}i_s - \frac{1}{\tau_r}\psi_r + \omega_r \begin{bmatrix} 0 & -1 \\ 1 & 0 \end{bmatrix} \psi_r, \quad (2b)$$

$$\frac{dv_{n,x}}{dt} = \frac{1}{2X_{dc}}\mathbf{o}^T s_x i_{s,x}, \quad x \in \{a, b, c\}, \quad (2c)$$

where the variables are the stator current  $i_s \in \mathbb{R}^2$  and the rotor flux  $\psi_r \in \mathbb{R}^2$  in the orthogonal  $\alpha\beta$ -frame, along with the three-phase neutral point potential  $v_{n,abc} \in \mathbb{R}^3$ .<sup>1</sup> The rotor angular speed  $\omega_r$  is considered to be a slowly varying parameter and, therefore, its dynamics are not modeled.

In (2), the transient stator and rotor time constants are given by  $\tau_s = X_r D / (R_s X_r^2 + R_r X_m^2)$  and  $\tau_r = X_r / R_r$ , respectively, where  $D = X_s X_r - X_m^2$ . Moreover,  $X_s = X_{ls} + X_m$  and  $X_r = X_{lr} + X_m$  are the stator and rotor self-reactances, respectively,  $X_{ls}$  and  $X_{lr}$  are the stator and rotor leakage reactances, respectively, and  $X_m$  is the mutual reactance. The resistances are  $R_s$  and  $R_r$  for the stator and rotor, respectively. Finally,  $I_2$  is the two-dimensional identity matrix, and  $\mathbf{o} = [1 \ -1 \ -1 \ 1]^T$ .

Let the system input be the *three-phase switching state*  $s_{abc} = [s_a^T s_b^T s_c^T]^T \in \{0, 1\}^{12}$ . The state  $\mathbf{x}$  comprises the stator current  $i_s$ , the rotor flux  $\psi_r$ , and the three-phase neutral point potentials  $v_{n,abc}$ , i.e.,  $\mathbf{x} = [i_s^T \ \psi_r^T \ v_{n,abc}^T]^T \in \mathbb{R}^7$ . Note that the state does not include the dynamics of the transformer and the rectifier, meaning that the phase- $x$  dc-link voltages,  $v_{dc,x}$ , are treated as measured external disturbances. Finally, the system output is  $\mathbf{y} = [i_s^T \ v_{n,abc}^T]^T \in \mathbb{R}^5$ . The dynamics of the system are then described by the continuous-time state-space model

$$\frac{d\mathbf{x}(t)}{dt} = \mathbf{F}(t)\mathbf{x}(t) + \mathbf{G}(t)s_{abc}(t), \quad (3a)$$

$$\mathbf{y}(t) = \mathbf{C}\mathbf{x}(t). \quad (3b)$$

For a detailed derivation of the matrices  $\mathbf{F}(t)$ ,  $\mathbf{G}(t)$ , and  $\mathbf{C}$ , the interested reader is referred to [12].

## III. OPTIMIZED PULSE PATTERNS WITH REDUCED DC-LINK RIPPLE

In this section, conventional quarter- and half-wave symmetric (QaHWS) and half-wave symmetric (HWS) OPPs are introduced and reviewed. Subsequently, the dc-link harmonic content of the five-level NPC H-bridge drive is analyzed, and OPPs that reduce the dc-link ripple are derived.

<sup>1</sup>Throughout the paper, variables in the three-phase  $abc$ -frame are denoted with the corresponding subscript, whereas variables in the  $\alpha\beta$ -frame are written without a subscript.

### A. Conventional Five-Level OPPs

Consider a  $2\pi$ -periodic single-phase switching signal  $u(\theta)$ ,  $\theta \in [0, 2\pi]$ , that can assume values  $u \in \{0, \pm 1, \pm 2\}$ . By imposing QaHWS, i.e.,

$$u(\pi - \theta) = u(\theta), \quad (4a)$$

$$u(\theta) = -u(\theta + \pi), \quad (4b)$$

the switching signal  $u(\theta)$  is defined by the  $d \in \mathbb{N}^+$  switching angles  $\alpha_i$ ,  $i \in \{1, 2, \dots, d\}$ , within the first quarter of the fundamental period, and the corresponding  $d + 1$  switch positions  $u_j$  with  $j \in \{0, 1, 2, \dots, d\}$ . It can be shown that such a switching signal we can be described with the Fourier series

$$u(\theta) = \frac{a_0}{2} + \sum_{n=1}^{\infty} (a_n \cos(n\theta) + b_n \sin(n\theta)), \quad (5)$$

where  $a_n$  and  $b_n$  are the Fourier coefficients of the  $n^{\text{th}}$  harmonic. These are given by

$$a_n = 0, \quad n = 0, 1, 2, \dots \quad (6a)$$

$$b_n = \begin{cases} \frac{4}{n\pi} \sum_{i=1}^d \frac{\Delta u_i}{2} \cos(n\alpha_i), & n = 1, 3, 5, \dots \\ 0, & n = 2, 4, 6, \dots \end{cases} \quad (6b)$$

where  $\Delta u_i \in \{-1, 1\}$  with  $i \in \{1, 2, \dots, d\}$  is the switching transition between two consecutive switch positions  $u_i$ , i.e.,

$$\Delta u_i = u_i - u_{i-1}. \quad (7)$$

To increase the degrees of freedom in the OPP optimization problem, it is beneficial to drop the assumption of quarter-wave symmetry (see (4a)), resulting in a HWS switching signal. Consequently, the Fourier coefficients in (5) are

$$a_n = \begin{cases} -\frac{2}{n\pi} \sum_{i=1}^{2d} \frac{\Delta u_i}{2} \sin(n\alpha_i), & n = 1, 3, 5, \dots \\ 0, & n = 0, 2, 4, 6, \dots \end{cases} \quad (8a)$$

$$b_n = \begin{cases} \frac{2}{n\pi} \sum_{i=1}^{2d} \frac{\Delta u_i}{2} \cos(n\alpha_i), & n = 1, 3, 5, \dots \\ 0, & n = 2, 4, 6, \dots \end{cases} \quad (8b)$$

Note that when HWS switching signals are considered, the OPP is defined by the  $2d$  switching angles and the corresponding  $2d + 1$  switch positions within the first half of the fundamental period. Regardless of the imposed symmetries, the amplitude of the  $n^{\text{th}}$  switching signal harmonic is given by  $\hat{u}_n = \sqrt{a_n^2 + b_n^2}$ . This implies that for the five-level NPC H-bridge inverter, the corresponding voltage harmonic is  $\hat{v}_n = V_{\text{dc}} \hat{u}_n$ , with  $V_{\text{dc}}$  being the nominal dc-link voltage.

Conventional OPPs aim to minimize the load current harmonic content. For this reason, the TDD of the load current

$$I_{\text{TDD}} = \frac{1}{\sqrt{2}I_{\text{nom}}} \sqrt{\sum_{n \neq 1} \hat{i}_n^2} \quad (9)$$

is utilized as a performance metric. In (9),  $I_{\text{nom}}$  is the rms value of the nominal current, while  $\hat{i}_n$  is the amplitude of the  $n^{\text{th}}$  current harmonic. Assuming that the inverter is connected to an induction machine (IM) with a total leakage reactance

of  $X_\sigma$  (the stator resistance is neglected), the  $n^{\text{th}}$  current harmonic is given by

$$\hat{i}_n = \frac{\hat{v}_n}{n\omega_1 X_\sigma} \quad (10)$$

with  $\omega_1$  being the fundamental angular frequency. Thus, by substituting the  $n^{\text{th}}$  voltage harmonic  $\hat{v}_n$  into (10), the current TDD defined in (9) becomes

$$I_{\text{TDD}} = \frac{V_{\text{dc}}}{\underbrace{\sqrt{2}I_{\text{nom}}\omega_1 X_\sigma}_C} \sqrt{\sum_{n \neq 1} \left(\frac{\hat{u}_n}{n}\right)^2}. \quad (11)$$

When the minimization of (11) is of interest, the term  $C$  can be discarded, as it is merely a system-dependent scaling factor of the current TDD. Therefore, while it affects the optimal value, it does not affect the optimizer. The same reasoning applies to the square root. For this reason, the objective function for the OPP optimization problem is defined as

$$J = \sum_{n=5,7,11,\dots} \left(\frac{\hat{u}_n}{n}\right)^2. \quad (12)$$

It is important to note that even harmonics ( $n = 2, 4, 6, \dots$ ) are not considered in (12) since these are zero due to the imposed symmetry (see (6) and (8)). Moreover, assuming a balanced load with a floating star point, the common-mode harmonics—i.e., the harmonic orders which are integer multiples of three ( $n = 3, 6, 9, \dots$ )—are also omitted since they do not drive harmonic current.

With the above analysis, the conventional QaHWS OPP optimization problem is

$$\begin{aligned} & \underset{\alpha_d, \mathbf{u}_d}{\text{minimize}} && \sum_{n=5,7,11,\dots} \frac{b_n^2}{n^2} \\ & \text{subject to} && b_1 = m \\ & && 0 < \alpha_1 < \alpha_2 < \dots < \alpha_d < \frac{\pi}{2} \\ & && u_i \in \{0, 1, 2\}, \quad |u_i - u_{i-1}| = 1 \\ & && \forall i \in \{1, \dots, d\}, \end{aligned} \quad (13)$$

with  $\alpha_d = [\alpha_1 \ \alpha_2 \ \dots \ \alpha_d]^T$  and  $\mathbf{u}_d = [u_0 \ u_1 \ \dots \ u_d]^T$ . In the above, the first constraint ensures that the magnitude of the fundamental component equals the desired modulation index  $m \in [0, 4/\pi]$ , while the remaining constraints guarantee that the resulting switching signal is feasible.

Similarly, for an HWS switching signal, the OPP optimization problem is

$$\begin{aligned} & \underset{\alpha_{2d}, \mathbf{u}_{2d}}{\text{minimize}} && \sum_{n=5,7,11,\dots} \frac{a_n^2 + b_n^2}{n^2} \\ & \text{subject to} && a_1 = 0, \ b_1 = m \\ & && 0 < \alpha_1 < \alpha_2 < \dots < \alpha_{2d} < \pi \\ & && u_i \in \{0, 1, 2\}, \quad |u_i - u_{i-1}| = 1 \\ & && \forall i \in \{1, \dots, 2d\}, \end{aligned} \quad (14)$$

with  $\alpha_{2d} = [\alpha_1 \ \alpha_2 \ \dots \ \alpha_{2d}]^T$  and  $\mathbf{u}_d = [u_0 \ u_1 \ \dots \ u_{2d}]^T$ . In contrast to the QaHWS optimization problem (13), the first constraint in (14) enforces not only that the magnitude of the

fundamental component equals the modulation index  $m$ , but also that its phase is zero.

### B. Dc-Link Harmonic Analysis

As explained in Section II, each phase of the five-level NPC H-bridge drive consists of a 12-pulse rectifier supplying an independent dc link, which, in turn, feeds a three-level H-bridge module (see Fig. 1). This implies that—from the point of view of the dc link—the load draws single-phase power. As a result, a predominant second harmonic appears in the dc-link voltage of each phase.

By assuming a sinusoidal load current and that a QaHWS or HWS OPP is used, the instantaneous power drawn from the dc link of a single phase is approximately<sup>2</sup>

$$p_{\text{load}}(t) \approx I_{\text{load}} \sin(\omega_1 t + \phi) \left( V_{\text{dc}} \sum_{n=1,3,5,\dots} (a_n \cos(n\theta) + b_n \sin(n\theta)) \right), \quad (15)$$

with  $I_{\text{load}}$  being the magnitude of the load current, and  $\phi$  the displacement angle, i.e., the angle between the inverter voltage and the load current. Assuming that the rectifier supplies the dc link with power  $p_{\text{supp}}(t)$ , the dc-link voltage can be expressed based on the energy stored in the dc-link capacitors as

$$v_{\text{dc}}(t) = \sqrt{\frac{1}{X_{\text{dc}}} \left( \int_0^t p_{\text{supp}}(\tau) d\tau - \int_0^t p_{\text{load}}(\tau) d\tau \right)}. \quad (16)$$

In the following, we focus on the capacitor energy term in (16) related to the load side, i.e.,  $e_{\text{dc,load}}(t) = \int_0^t p_{\text{load}}(\tau) d\tau$ . Substituting (15) into  $e_{\text{dc,load}}$  and evaluating the integral gives

$$\begin{aligned} e_{\text{dc,load}}(t) &= \frac{I_{\text{load}} V_{\text{dc}}}{\omega_1} \left( \frac{1}{2} t \cos(\phi) - \frac{b_1}{4} \sin(2\omega_1 t + \phi) \right. \\ &+ \sum_{n=3,5} \frac{a_n}{2(n-1)} \cos(-(n-1)\omega_1 t + \phi) \\ &- \sum_{n=3,5} \frac{a_n}{2(n+1)} \cos((n+1)\omega_1 t + \phi) \\ &- \sum_{n=3,5} \frac{b_n}{2(n-1)} \sin(-(n-1)\omega_1 t + \phi) \\ &\left. - \sum_{n=3,5} \frac{b_n}{2(n+1)} \sin((n+1)\omega_1 t + \phi) \right). \quad (17) \end{aligned}$$

As can be seen, a term that increases linearly with time  $\frac{1}{2} t \cos(\phi)$  and even-order harmonic components are injected into the dc link from the load side. The linear term has to be compensated for by the supply side, i.e.,  $p_{\text{supp}}$ , as otherwise the dc-link voltage would drift uncontrollably (see (16)). The harmonic terms, however, cannot be fully compensated

<sup>2</sup>For a more accurate description of the instantaneous power, one would have to account for the harmonic content of both the dc-link voltage and the load current. However, as these harmonics are of significantly smaller magnitude than the dc component of the dc-link voltage and the fundamental component of the load current, respectively, they are neglected.

for with a first-quadrant rectifier such as the 12-pulse diode rectifier considered in this work.

Considering only the harmonic terms in (17), the harmonic content of the capacitor energy originating from the load side,  $\Delta e_{\text{dc,load}}$ , can be expressed as the (scaled) Fourier series

$$\Delta e_{\text{dc,load}}(t) = \frac{I_{\text{load}} V_{\text{dc}}}{2\omega_1} \left( \sum_{n=1,3,5,\dots} a_{n+1,\text{dc}} \cos((n+1)\omega_1 t) + b_{n+1,\text{dc}} \sin((n+1)\omega_1 t) \right), \quad (18)$$

with the Fourier coefficients

$$\begin{aligned} a_{n+1,\text{dc}} &= \frac{-a_n \cos(\phi) - b_n \sin(\phi) + a_{n+2} \cos(\phi) - b_{n+2} \sin(\phi)}{n+1} \\ b_{n+1,\text{dc}} &= \frac{a_n \sin(\phi) - b_n \cos(\phi) + a_{n+2} \sin(\phi) + b_{n+2} \cos(\phi)}{n+1}. \end{aligned}$$

With the above, the dc-link voltage (16) can be written as

$$v_{\text{dc}}(t) = \left\{ \frac{1}{X_{\text{dc}}} \left( \int_0^t p_{\text{supp}}(\tau) d\tau - \frac{I_{\text{load}} V_{\text{dc}}}{\omega_1} \frac{1}{2} t \cos(\phi) - \Delta e_{\text{dc,load}}(t) \right) \right\}^{\frac{1}{2}}. \quad (19)$$

Note that the effect of the power supplied by the 12-pulse rectifier  $p_{\text{supp}}$  on the harmonic content of the dc-link voltage is not explicitly known in (19). Hence, it may interact with the harmonics originating from the load side, i.e.,  $\Delta e_{\text{dc,load}}$ . Nevertheless, it is assumed that the power supplied by the rectifier fully compensates for the linear term in (19) such that the average dc-link voltage remains constant.

### C. Optimization Problem

To improve the drive performance, this work proposes OPPs that minimize the harmonic content of the dc-link voltage. Although the interaction between the supply and the load sides in (19) is unclear the use of a 36-pulse rectifier implies that the harmonic content introduced by the supply is negligible compared to dominant second harmonic generated by the load. For this reason, the proposed OPPs account only for the harmonics originating from the load side, quantified by the square root of the sum of the squared capacitor energy harmonics, i.e.,

$$\Delta e_{\text{dc}} = \sqrt{\sum_{n=1,3,5,\dots} (\Delta \hat{e}_{n+1,\text{dc}})^2}, \quad (20)$$

where the amplitude of the  $(n+1)^{\text{th}}$  harmonic  $\Delta \hat{e}_{n+1,\text{dc}}$  is

$$\Delta \hat{e}_{n+1,\text{dc}} = \sqrt{a_{n+1,\text{dc}}^2 + b_{n+1,\text{dc}}^2}. \quad (21)$$

With the two relationships above, the objective function that approximately captures the dc-link voltage ripple is

$$J_{\text{dc}} = \sum_{n=1,3,5,\dots} a_{n+1,\text{dc}}^2 + b_{n+1,\text{dc}}^2. \quad (22)$$

Similarly to conventional OPPs, the square root in (20) does not affect the optimizer and is therefore omitted in (22). Hence, minimizing  $J_{dc}$  is equivalent to minimizing the capacitor energy harmonic content injected into the dc link by the load.

With function (22), the proposed OPP optimization problem can be formulated. First, to facilitate greater mitigation of the dc-link voltage harmonics, HWS OPPs are computed such that their phase is also manipulated. Moreover, to avoid compromising the stator current quality, the current TDD, quantified by the objective function (12), is bounded with the inequality constraint

$$\sum_{n=5,7,11,\dots} \frac{a_n^2 + b_n^2}{n^2} \leq \epsilon J^*(\alpha_{2d}, \mathbf{u}_{2d}). \quad (23)$$

In constraint (23),  $J^*$  is the optimal value of problem (14), and  $\epsilon \geq 1$  is a tuning parameter. By appropriately selecting its value, the trade-off between dc-link voltage harmonic content reduction and load current TDD can be adjusted. For example, decreasing  $\epsilon$  enables greater reduction of the load current TDD but at the expense of increased dc-link voltage ripple. Therefore, constraint (23) provides the controller designer with a degree of freedom to fine-tune the balance between the load current TDD and the dc-link voltage ripple.

Given the above, the OPP optimization problem that achieves a favorable trade-off between low dc-link voltage harmonics and stator current TDD is formulated as

$$\begin{aligned} & \underset{\alpha_{2d}, \mathbf{u}_{2d}}{\text{minimize}} && \sum_{n=1,3,5,\dots} a_{n+1,dc}^2 + b_{n+1,dc}^2 \\ & \text{subject to} && \sum_{n=5,7,11,\dots} \frac{a_n^2 + b_n^2}{n^2} < \epsilon J^*(\alpha_{2d}, \mathbf{u}_{2d}) \\ & && a_1 = 0, b_1 = m \\ & && 0 < \alpha_1 < \alpha_2 < \dots < \alpha_{2d} < \pi \\ & && u_i \in \{0, 1, 2\}, \quad |u_i - u_{i-1}| = 1 \\ & && \forall i \in \{1, \dots, 2d\}. \end{aligned} \quad (24)$$

#### IV. S-GP<sup>3</sup>C FOR THE FIVE-LEVEL NPC H-BRIDGE MV DRIVE SYSTEM

The objective of the S-GP<sup>3</sup>C strategy [9] is to regulate the output  $\mathbf{y}$  along its *optimal* reference trajectory  $\mathbf{y}_{\text{ref}}$  by manipulating the OPPs computed in Section III in real time.

To do so, let

$$\mathbf{t}_{x,\text{ref}} = [t_{x1,\text{ref}} \ t_{x2,\text{ref}} \ \dots \ t_{xz_x,\text{ref}}]^T \in \mathbb{R}^{z_x} \quad (25)$$

be a vector containing the  $z_x \in \mathbb{N}^+$  nominal switching time instants of the OPP in phase  $x$  within the time window  $T_p = N_p T_s$ , i.e., the prediction horizon, where  $N_p$  is the number of prediction steps and  $T_s$  the sampling interval. S-GP<sup>3</sup>C computes the corresponding *optimally* modified switching time instants in each phase

$$\mathbf{t}_x = [t_{x1} \ t_{x2} \ \dots \ t_{xz_x}]^T \in \mathbb{R}^{z_x}, \quad (26)$$

such that the output tracking error is minimized within  $T_p$ .

To this end, the output reference  $\mathbf{y}_{\text{ref}}$  is sampled at the  $z_p \in$

$\mathbb{N}^+$  nominal ‘‘pivotal’’ switching time instants

$$\mathbf{t}_{p,\text{ref}} = [t_{p1,\text{ref}} \ t_{p2,\text{ref}} \ \dots \ t_{pz_p,\text{ref}}]^T \in \mathbb{R}^{z_p}, \quad (27)$$

while the output  $\mathbf{y}$  is predicted at the corresponding modified pivotal time instants

$$\mathbf{t}_p = [t_{p1} \ t_{p2} \ \dots \ t_{pz_p}]^T \in \mathbb{R}^{z_p}. \quad (28)$$

These pivotal time instants appear in the OPP for all three phases. However, it is important to note that no switching event occurs at these time instants, i.e.,  $\mathbf{s}_x(t_{p\kappa,\text{ref}})^- \equiv \mathbf{s}_x(t_{p\kappa,\text{ref}})^+$  with  $\kappa \in \{1, 2, \dots, z_p\}$ ; see [9] for more details. Thus, the nominal (or modified) switching time instants considered in the control problem result by aggregating the vectors  $\mathbf{t}_{x,\text{ref}}$  (or  $\mathbf{t}_x$ ) and  $\mathbf{t}_{p,\text{ref}}$  (or  $\mathbf{t}_p$ ) into a single vector  $\tilde{\mathbf{t}}_{x,\text{ref}} \in \mathbb{R}^{z_x+z_p}$  (or  $\tilde{\mathbf{t}}_x \in \mathbb{R}^{z_x+z_p}$ ), where the combined switching time instants are sorted in a chronological order.

For S-GP<sup>3</sup>C to minimize the reference tracking error, the effect of the phase- $x$  switching state  $\mathbf{s}_x$ —as defined by the OPP in use—on the evolution of the system over each time interval of the horizon  $\Delta \tilde{\mathbf{t}}_{x\ell,\text{ref}} = \tilde{\mathbf{t}}_{x\ell+1,\text{ref}} - \tilde{\mathbf{t}}_{x\ell,\text{ref}}$ ,  $\ell \in \{0, 1, 2, \dots, z_p+z_x\}$ , needs to be determined. To this aim, the corresponding (constant) output gradients are computed according to

$$\mathbf{m}^x(\tilde{\mathbf{t}}_{x\ell,\text{ref}}) = \frac{\mathbf{y}^x(\tilde{\mathbf{t}}_{x\ell+1,\text{ref}}) - \mathbf{y}^x(\tilde{\mathbf{t}}_{x\ell,\text{ref}})}{\Delta \tilde{\mathbf{t}}_{x\ell,\text{ref}}}. \quad (29)$$

With the gradients  $\mathbf{m}^x$ , the objective function of the S-GP<sup>3</sup>C algorithm is written as

$$J_{\text{S-GP}^3\text{C}} = \|\mathbf{r} - \mathbf{M}\mathbf{t}\|_{\tilde{\mathbf{Q}}}^2 + \lambda_t \|\Delta \mathbf{t}\|_2^2, \quad (30)$$

where the vector  $\mathbf{t}$  collects the modified switching and pivotal time instants in all the three phases, i.e.,

$$\mathbf{t} = [\mathbf{t}_a \ \mathbf{t}_b \ \mathbf{t}_c \ \mathbf{t}_p]^T \in \mathbb{R}^{z_a+z_b+z_c+z_p}. \quad (31)$$

The vector  $\mathbf{r}$  depends on the reference values  $\mathbf{y}_{\text{ref}}$  and the measurements of the output, and  $\mathbf{M} \in \mathbb{R}^{n_y z_p \times z_a+z_b+z_c+z_p}$  is a matrix consisting of the gradients  $\mathbf{m}^x$  with which the controlled variables evolve over the prediction horizon  $T_p$ . The entries  $q_{i_s} > 0$  and  $q_{v_n} > 0$  of the block diagonal weighting matrix  $\tilde{\mathbf{Q}}$  prioritize the tracking accuracy between the stator current  $\mathbf{i}_s$  and the three-phase NP potential  $\mathbf{v}_{n,abc}$ , respectively. The second term in (30) is added to penalize changes in the nominal OPP switching time instants, i.e.,

$$\Delta \mathbf{t} = \mathbf{t}_{\text{ref}} - \mathbf{t} \quad (32)$$

through the weighting factor  $\lambda_t > 0$ , with

$$\mathbf{t}_{\text{ref}} = [\mathbf{t}_{a,\text{ref}} \ \mathbf{t}_{b,\text{ref}} \ \mathbf{t}_{c,\text{ref}} \ \mathbf{t}_{p,\text{ref}}]^T \in \mathbb{R}^{z_a+z_b+z_c+z_p}. \quad (33)$$

With (30), the S-GP<sup>3</sup>C optimal control problem is

$$\begin{aligned} & \underset{\mathbf{t}}{\text{minimize}} && \|\mathbf{r} - \mathbf{M}\mathbf{t}\|_{\tilde{\mathbf{Q}}}^2 + \lambda_t \|\Delta \mathbf{t}\|_2^2 \\ & \text{subject to} && t_0 \leq \tilde{t}_{a1} \leq \tilde{t}_{a2} \leq \dots \leq \tilde{t}_{a\tilde{z}_a} \leq t_0 + T_p \\ & && t_0 \leq \tilde{t}_{b1} \leq \tilde{t}_{b2} \leq \dots \leq \tilde{t}_{b\tilde{z}_b} \leq t_0 + T_p \\ & && t_0 \leq \tilde{t}_{c1} \leq \tilde{t}_{c2} \leq \dots \leq \tilde{t}_{c\tilde{z}_c} \leq t_0 + T_p. \end{aligned} \quad (34)$$

TABLE I  
RATED VALUES OF THE INDUCTION MACHINE

Parameter	Symbol	SI value
Voltage	$V_R$	5389 V
Current	$I_R$	1485 A
Apparent power	$S_R$	12 MVA
Stator frequency	$\omega_{sR}$	$2\pi 50$ rad/s
Rotational speed	$\omega_{mR}$	1490 rpm

TABLE II  
SYSTEM PARAMETER VALUES IN THE P.U. SYSTEM

Parameter	Symbol	p.u.
Stator resistance	$R_s$	0.0054
Rotor resistance	$R_r$	0.0066
Stator leakage reactance	$X_{ls}$	0.1299
Rotor leakage reactance	$X_{lr}$	0.1105
Mutual reactance	$X_m$	4.3496
Nominal dc-link voltage	$V_{dc}$	0.9620
Dc-link capacitor reactance	$X_{dc}$	4.4464

The optimization problem (34) is solved in real time at each iteration of the controller, yielding the *optimally* modified switching time instants  $t^*$ . As can be seen, the to-be-computed switching time instants must retain their chronological order within each phase. Nevertheless, following the receding horizon principle of MPC, only the switching time instants that fall within the first sampling interval  $T_s$  of the prediction horizon  $T_p$  are applied to the inverter, introducing a feedback loop. Subsequently, the prediction horizon is shifted forward by one sampling interval and the algorithm is restarted. For a detailed description of the S-GP<sup>3</sup>C algorithm and the definitions of  $r$ ,  $M$ , and  $\tilde{Q}$ , the interested reader is referred to [9].

## V. PERFORMANCE EVALUATION

The performance of the proposed control scheme is assessed through simulations on a 12 MVA drive (see Fig. 1). The rated values of the IM are provided in Table I, while Table II summarizes the system parameters. The total leakage reactance of the machine is  $X_\sigma = 0.24$  p.u. Regarding the controller parameters, the sampling interval is  $T_s = 50 \mu\text{s}$  and a 10-step ( $N_p = 10$ ) prediction horizon is used. The output weighting coefficients are  $q_{i_s} = 1$  and  $q_{v_n} = 10$ , while the controller effort weight is  $\lambda_t = 10^5$ . A five-level OPP with a pulse number  $d = 5$  is used, implying an average device switching frequency  $f_{sw} = 125$  Hz for operation at rated speed. The modulation index is  $m = 1.05$  and  $\epsilon = 2.1$ . Finally, all results are shown in the per unit (p.u.) system.

### A. Trade-Off Between Dc-Link Voltage Ripple and Current TDD

To quantify the effectiveness of the proposed OPPs, a comparison between conventional QaHWS OPPs (13), conventional HWS OPPs (14), and the proposed OPPs (24) is shown in Fig. 2. All OPPs are computed for a modulation

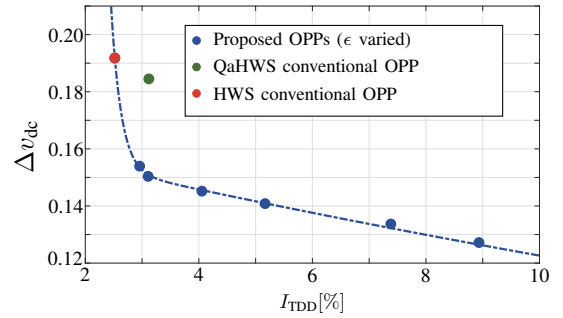


Fig. 2. Comparison of the proposed OPPs with conventional OPPs for  $m = 1.05$ . The tuning parameter  $\epsilon$  is varied in the range  $\epsilon \in [1, 30]$ .

index  $m = 1.05$ , which is typical for an MV drive at nominal operating conditions. For the proposed OPPs, the tuning parameter  $\epsilon$  is varied in the range  $[1, 30]$ .

As can be seen, the proposed OPPs achieve a favorable trade-off between dc-link voltage ripple and stator current TDD through the adjustment of the tuning parameter  $\epsilon$ . For example, compared to the conventional QaHWS OPPs, the proposed OPPs can reduce the peak-to-peak dc-link voltage ripple by up to 20% without increasing the stator current TDD. When compared to the conventional HWS OPPs, the proposed OPPs achieve the same current TDD and peak-to-peak dc-link voltage ripple for  $\epsilon = 1$  due to the constraint (23). For larger values of  $\epsilon$ , however, the proposed OPPs yield a lower dc-link voltage ripple, albeit at the cost of a higher stator current TDD compared to the conventional HWS OPPs.

### B. Steady-State Performance

The steady-state performance of the drive system at rated torque is shown in Fig. 3. As can be seen in Figs. 3(b) and 3(a), the proposed control strategy achieves excellent stator current—and, consequently, electromagnetic torque—reference tracking despite the oscillations in the dc-link voltages. This indicates that S-GP<sup>3</sup>C can effectively compensate for external disturbances. As a result, the stator current quality is very good, as reflected by the TDD of only 3.69%, see Fig. 3(f). Moreover, thanks to the symmetry properties of the baseline OPP, the harmonic power is concentrated at the odd non-triplen integer multiples of the fundamental frequency. Additionally, as shown in Fig. 3(d), the three-phase neutral point potentials are kept balanced and close to zero. Finally, owing to the use of the proposed OPP, the peak-to-peak ripple of the dc-link voltage  $\Delta v_{dc}$  is only 0.15 p.u., i.e., the favorable trade-off between current TDD and dc-link voltage ripple is retained by the controller, see Fig. 3(e).

To further assess the performance of the proposed control method, it is benchmarked against field-oriented control (FOC) with CB-PWM. The performance of FOC with CB-PWM is shown in Fig. 4. As can be seen in Fig. 4(b), the stator current has significantly higher ripple under FOC than with the proposed method, leading to a TDD of 5.75%, i.e., over 55% higher than that achieved with S-GP<sup>3</sup>C. Moreover, the harmonic power is primarily concentrated in the low-order harmonics, such as the 5<sup>th</sup> and 7<sup>th</sup>. As for the peak-to-peak

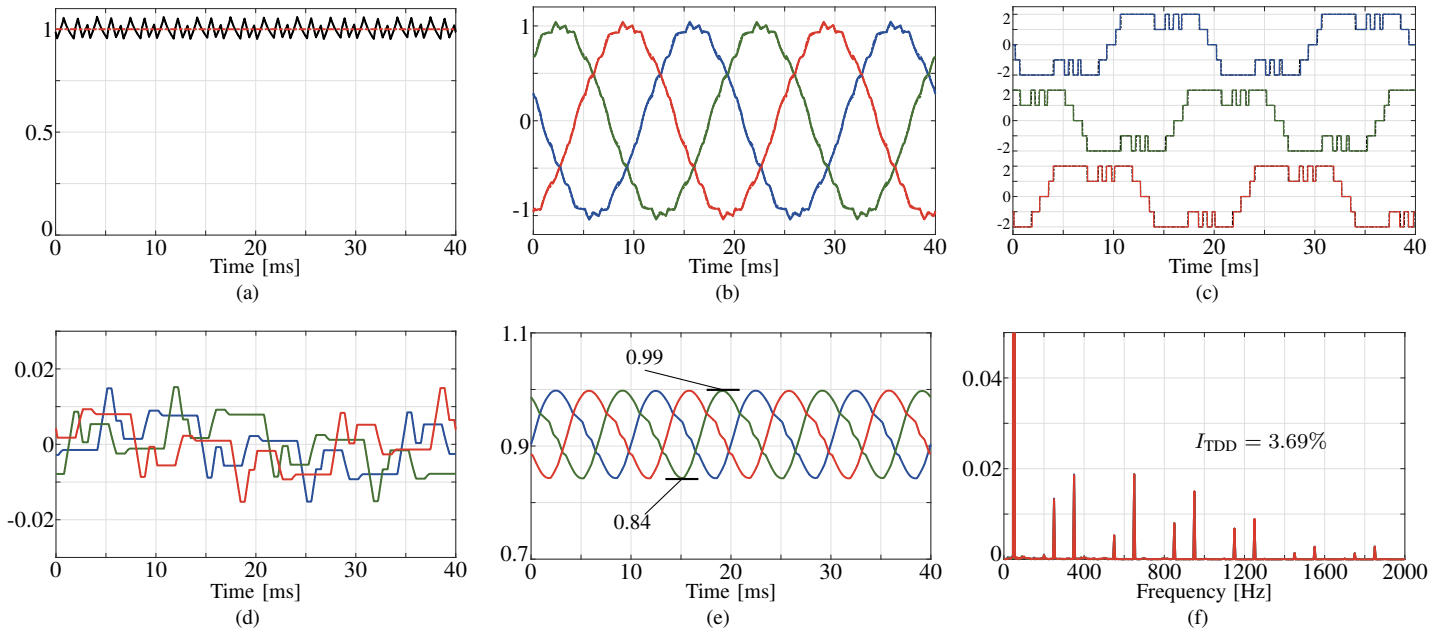


Fig. 3. Steady-state performance of the proposed control strategy at nominal operating conditions. (a) Electromagnetic torque  $T_e$  (black line) and its reference (red dash-dotted line); (b) three-phase stator currents  $i_{s,abc}$  (solid lines) and their references (dash-dotted lines); (c) three-phase (modified) switching pattern (solid lines) and nominal OPP (dash-dotted lines); (d) three-phase NP potentials  $v_{n,abc}$  (solid lines); (e) three-phase dc-link voltages  $v_{dc,abc}$ ; (f) stator current spectrum.

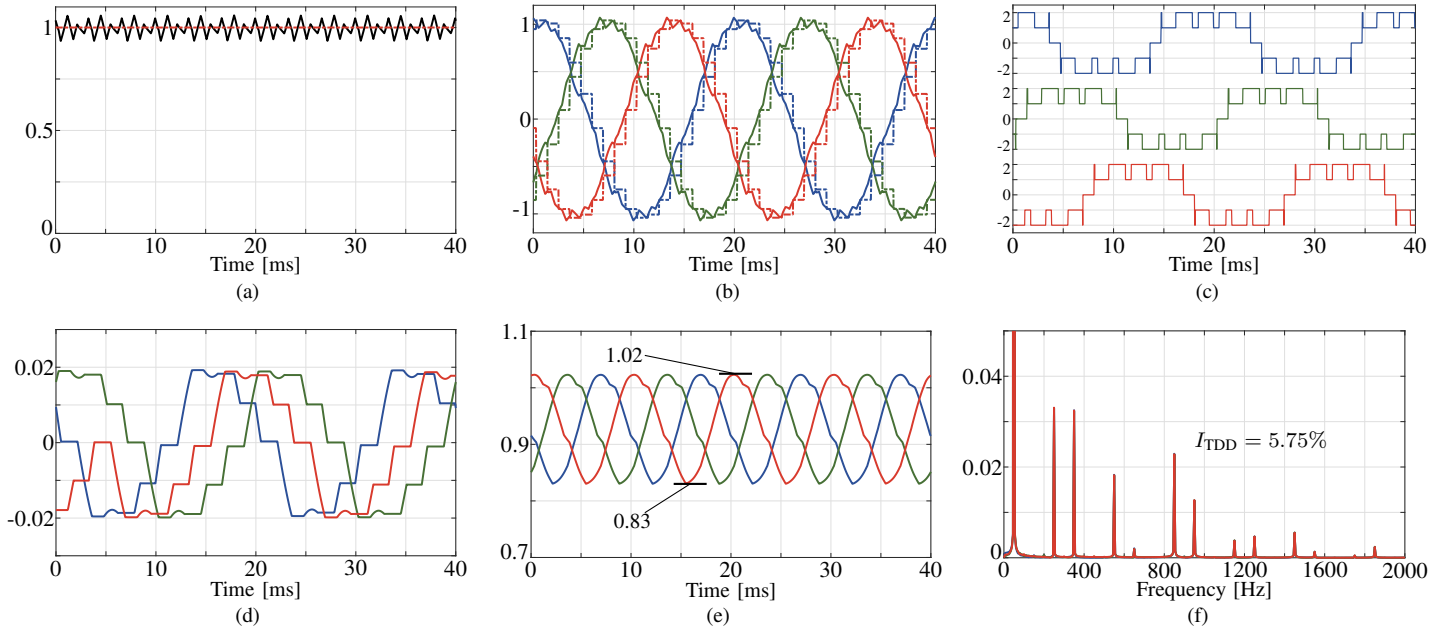


Fig. 4. Steady-state performance of FOC with CB-PWM at nominal operating conditions. (a) Electromagnetic torque  $T_e$  (black line) and its reference (red dash-dotted line); (b) three-phase stator currents  $i_{s,abc}$  (solid lines) and their references (dash-dotted lines); (c) three-phase switching pattern; (d) three-phase NP potentials  $v_{n,abc}$  (solid lines); (e) three-phase dc-link voltages  $v_{dc,abc}$ ; (f) stator current spectrum.

dc-link voltage ripple, it is 0.20 p.u., which is 25% higher than the ripple achieved with S-GP<sup>3</sup>C using the proposed OPPs.

### C. Transient Performance

The transient performance of the proposed control scheme is shown in Fig. 5. In the examined scenario, the electromagnetic torque reference is stepped down from its nominal value, i.e.,  $T_{e,ref} = 1$  p.u., to  $T_{e,ref} = 0.2$  p.u. at time  $t = 10$  ms. As

observed, the controller quickly regulates the stator current along its new reference—generated based on the demanded torque—by drastically modifying the nominal OPP. More specifically, by inverting the voltage in the red and blue phases (see Fig. 5(c)), a very fast transient response is achieved. During a torque step down, the stator current decreases quickly and the excess energy is fed back to the dc links. This

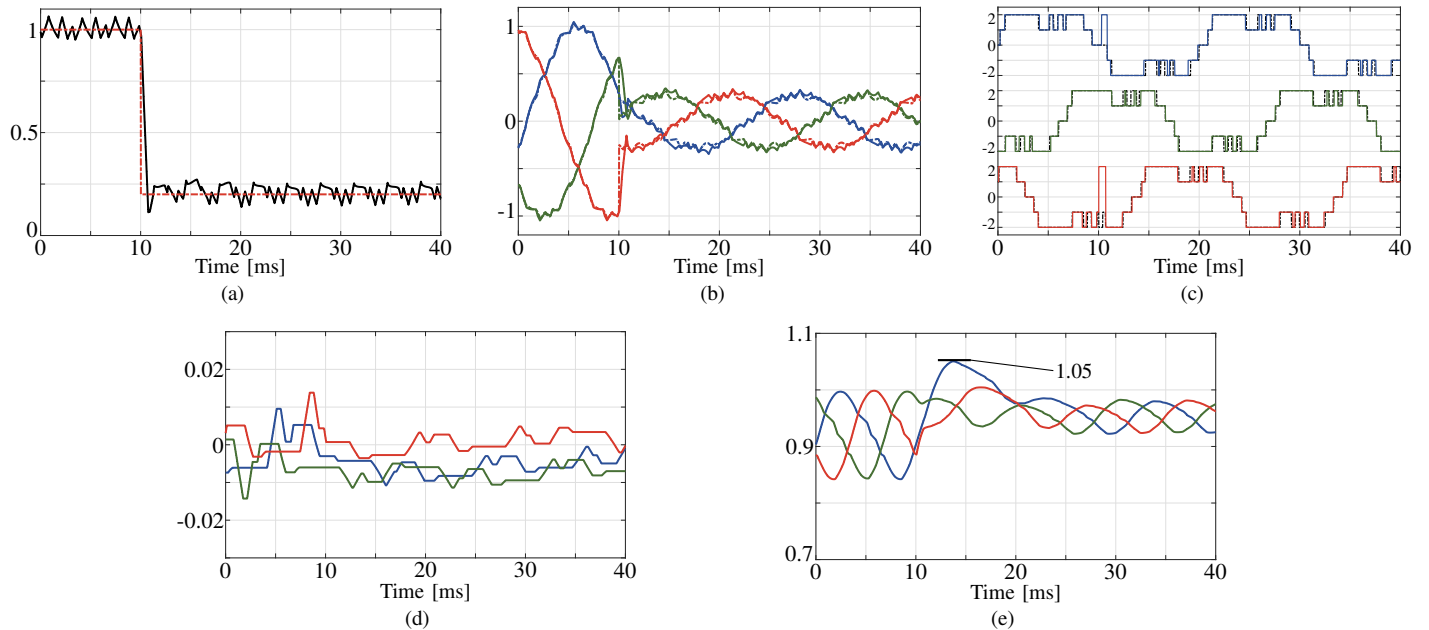


Fig. 5. Transient performance of the proposed control strategy during a step-down change in the torque reference. (a) Electromagnetic torque  $T_e$  (black line) and its reference (red dash-dotted line); (b) three-phase stator currents  $i_{s,abc}$  (solid lines) and their references (dash-dotted lines); (c) three-phase (modified) switching pattern (solid lines) and nominal OPP (dash-dotted lines); (d) three-phase NP potentials  $v_{n,abc}$  (solid lines); (e) three-phase dc-link voltages  $v_{dc,abc}$ .

phenomenon causes notable deviations in the dc-link voltages, as shown in Fig. 5(e). However, S-GP<sup>3</sup>C handles these disturbances effectively by independently modifying each phase of the nominal OPP, thus compensating for the dc-link voltage variations.

## VI. CONCLUSION

This paper adapted the S-GP<sup>3</sup>C method [9] to the five-level NPC H-bridge MV drive and enhanced it with OPPs that effectively reduce the dc-link voltage ripple while maintaining very low current TDD values. By analyzing the harmonic content of the dc-link voltage, an OPP optimization problem was formulated to minimize its harmonic content. In addition, by constraining the load current TDD in the same problem, a trade-off between load current TDD and dc-link voltage ripple reduction is achieved. The results demonstrate that the proposed OPPs can effectively reduce the peak-to-peak dc-link voltage ripple without significantly compromising the stator current quality. Additionally, by utilizing the S-GP<sup>3</sup>C method to manipulate the proposed OPPs in real time, excellent steady-state and transient performance is achieved, while preserving the beneficial qualities of the proposed OPPs. As a result, the proposed approach outperforms conventional modulation and control methods, such as FOC with CB-PWM.

## ACKNOWLEDGEMENT

This work was supported by the Research Council of Finland.

## REFERENCES

[1] K. Gupta, R. Ranjan, P. Bhatnagar, L. Sahu, and S. Jain, "Multilevel inverter topologies with reduced device count: A review," *IEEE Trans. Power Electron.*, vol. 31, no. 1, Jan. 2016.

[2] C. Wu, W. Lau, and H. Chung, "A five-level neutral-point-clamped H-bridge PWM inverter with superior harmonics suppression: A theoretical analysis," in *Proc. IEEE Int. Symp. Circuits Syst.*, Orlando, FL, USA, May/Jun. 1999, pp. V-198-V-201.

[3] J. Shen, S. Schröder, J. Gao, and B. Qu, "Impact of dc-link voltage ripples on the machine-side performance in NPC H-bridge topology," *IEEE Trans. Ind. Appl.*, vol. 52, no. 4, pp. 3212-3223, Jul./Aug. 2016.

[4] J. Shen, S. Schröder, H. Stage, and R. W. D. Doncker, "Impact of modulation schemes on the power capability of high-power converters with low pulse ratios," *IEEE Trans. Power Electron.*, vol. 29, no. 11, pp. 5696-5705, Nov. 2014.

[5] G. S. Buja and G. B. Indri, "Optimal pulsewidth modulation for feeding ac motors," *IEEE Trans. Ind. Appl.*, vol. IA-13, no. 1, pp. 38-44, Jan./Feb. 1977.

[6] G. S. Buja, "Optimum output waveforms in PWM inverters," *IEEE Trans. Ind. Appl.*, vol. IA-16, no. 6, pp. 830-836, Nov./Dec. 1980.

[7] A. K. Rathore, J. Holtz, and T. Boller, "Synchronous optimal pulsewidth modulation for low-switching-frequency control of medium-voltage multilevel inverters," *IEEE Trans. Ind. Electron.*, vol. 57, no. 7, pp. 2374-2381, Jul. 2010.

[8] T. Geyer, P. Karamanakos, and I. Koukoulou, "Optimized pulse patterns with bounded semiconductor losses," *IEEE Trans. Power Electron.*, vol. 39, no. 3, pp. 3233-3243, Mar. 2024.

[9] I. Hilden, P. Karamanakos, and T. Geyer, "Gradient-based predictive pulse pattern control with single phase formulation," in *Proc. IEEE Energy Convers. Congr. Expo.*, Philadelphia, PA, USA, Oct. 2025, pp. 1-8.

[10] S. Kouro, M. A. Perez, J. Rodríguez, A. M. Llor, and H. A. Young, "Model predictive control: MPC's role in the evolution of power electronics," *IEEE Ind. Electron. Mag.*, vol. 9, no. 4, pp. 8-21, Dec. 2015.

[11] J. Holtz, "The representation of ac machine dynamics by complex signal flow graphs," *IEEE Trans. Ind. Electron.*, vol. 42, no. 3, pp. 263-271, Jun. 1995.

[12] I. Hilden, P. Karamanakos, and T. Geyer, "Gradient-based predictive pulse pattern control with optimal active neutral point potential balancing for five-level medium-voltage drives," in *Proc. IEEE Energy Convers. Congr. Expo.*, Philadelphia, PA, USA, Oct. 2025, pp. 1-8.